Results from blade element momentum and RANS analyses of a practical full-scale horizontal axis tidal current turbine

Results from blade element momentum and RANS analyses of a practical full-scale horizontal axis tidal current turbine

Gareth I. Gretton[#1], David M. Ingram[#2], Ian G. Bryden[#3]
[#]*Institute for Energy Systems, School of Engineering, University of Edinburgh, UK*
[1]gareth.gretton@ed.ac.uk
[2]david.ingram@ed.ac.uk
[3]ian.bryden@ed.ac.uk

***Abstract*—Results are presented herein for the hydrodynamic behaviour of a practical full-scale horizontal axis tidal current turbine, based on blade element momentum (BEM) and Reynolds-averaged Navier Stokes (RANS) solutions. Power and thrust coefficients are predicted from both models and an analysis of the wake behind the turbine comes from the RANS solution. By practical, we make reference to a turbine rotor that has been conservatively designed with respect to in-service loads and which therefore features blade sections with large thickness to chord ratios (18% at tip to 55% at root).**

The BEM predictions were based on available experimental data and newly-generated data from Xfoil and RANS solutions. This highlighted the importance of using appropriate blade data. These RANS solutions for the blade sections, carried out using the open-source solver Code_Saturne, also functioned as a sub-component verification and validation exercise for the turbine simulations, carried out with the same solver and turbulence model.

All of these simulations were carried out as part of the PerAWaT project, commissioned by the Energy Technologies Institute, and are intended to provide data from which a parametric model of the wake can be determined, with the ultimate aim of being able to predict the performance of tidal current turbines in arrays.

***Index Terms*—Tidal current turbine, hydrodynamic performance, BEM, RANS, CFD**

I. Introduction

As noted in [1], the understanding of the hydrodynamic behaviour of arrays of tidal current turbines is a crucial step in their commercial development; without such understanding there will be an unacceptable level of uncertainty in the array performance and therefore a lack of investment. Appropriate computer models are therefore required, and in practice these must be based around some form of parameterization of the wake of a turbine. The present work, as part of the PerAWaT project, is concerned with the development of a RANS-based CFD model of an horizontal axis tidal current turbine, the results of which will be used to form such a parameterization.

The rotor geometry under consideration in the current work was provided to the project by Tidal Generation Limited (TGL) and is intended to be representative of practical designs. Specifically, this leads to relatively large thickness to chord ratios – varying from 18% at the tip to 55% at the root. All profiles are from the NACA 6-series. The geometry for the hub and nacelle was developed within the project and is based on basic engineering considerations, as outlined in § IV.

Prior to developing the aforementioned CFD model of the turbine, we elected to study the hydrodynamic behaviour of the blade sections used. This was beneficial for a number of reasons. First, there was no available data on the performance of the thicker sections used for the turbine rotor, this raising questions over the true performance of the rotor which had been designed using data for an 18% thick section; second, a number of ways of generating the section profiles were identified and we wished to investigate the significance of this; and third, a CFD analysis of the blade sections forms an important sub-component verification and validation exercise with regards to the turbine. We begin by discussing this work.

II. CFD results for the blade sections

A. Setup

The CFD setup for the present work on 2D blade sections has been strongly informed by previous work by the present authors, e.g. [2]. This previous work was completed using the commercial software Ansys CFX as opposed to Code_Saturne, but choices such as the turbulence model (SST-k-ω) and grid design have been maintained, thus providing a significant level of confidence in the current work. The boundary conditions specified were as follows: on the inlet the velocity, turbulence kinetic energy (k) and turbulence eddy dissipation rate (ϵ) were fixed; on the outlet the pressure was fixed; on the foil surfaces a no-slip condition was imposed; and on the 'front' and 'back' faces of the 1-volume thick 3D mesh, symmetry conditions were imposed to force a 2D flow. All grids used in the study were of C-type (or C-H-type in the case of the blunt trailing edge case) and had the far-field boundary 80 chord lengths from the foil.

All of these boundary conditions could be imposed directly through the graphical user interface of Code_Saturne with the exception of the turbulence parameters on the inlet. These were thus specified through a Fortran user subroutine. Values for k and ϵ were selected to produce a turbulence intensity of 0.1% and a length scale of $0.1\ \mathrm{m}$ at the foil, by allowing for

the decay from the inlet. The inlet velocity, and the constant values of the density and viscosity in the domain, were chosen to produce a Reynolds number of 3×10^6.

B. Verification

As noted above, the CFD setup for the current work on 2D blade sections, including the selection of the grid, is informed by previous work. This previous work focused on thinner blade sections than are typical of the present rotor geometry and so it was decided to carry out a grid verification exercise on the 63_x-430 section[1]. This exercise used three grids, termed 'coarse', 'medium' and 'fine'. The medium grid has 268 cells in the wrap-around direction (with 196 on the foil surface) and 82 cells in the wall-normal direction. The coarse and fine grids contain respectively half and double the number of cells in these two directions, thus giving one quarter and four times the number of cells in the mesh.

This study was carried out for angles of attack between zero and twenty degrees in two degree increments, with the results for the convergence of the lift and drag coefficients being given in Tables I and II. All of the parameters[2] given are as standard in the literature on grid convergence [e.g. 3, 4]. The conclusions that may be drawn are as follows. For the lift coefficient there is good convergence for moderate angles of attack (up to about 8-10°) and less good thereafter, with errors on the medium grid being low ($< 6\%$) for angles of attack up to 8°, rising notably thereafter. For the drag coefficient, the convergence is more problematic, with a number of cases showing oscillatory convergence ($-1 < R < 0$). Further, for the angles of attack which do show monotonic convergence, and where grid convergence indices can be calculated, there is no clear pattern, such as was observed for the lift coefficients. Given these inconclusive results, we therefore refer to past experience [2] which suggests that errors in the drag coefficient are likely to be higher than those for the lift coefficient.

With regards to the accuracy of the turbine simulations, and the ability to parameterize the wake, the most important parameter is C_T which is most strongly driven by the lift coefficient; the larger error in the drag is therefore of less importance. Also, the turbine is designed to operate at low to moderate angles of attack (below 8°), for which the errors in the lift are below 6%, and so simulations of the turbine near the design point should be correspondingly accurate. For tip speed ratios below the design point, where the angle of attack will be higher, we have to be cognizant of and accept larger errors.

Based on these results, we used the medium grid for the subsequent work on the blade sections.

C. Validation

Validation data for the NACA 6-series sections was found to be limited, with the only source being Abbott and von Doenhoff [5]. This unfortunately did not include sections thicker than 21% and so the validation exercise was limited to the 18% and 21% sections used for the blade. These show largely similar behaviour and so we show only the results for the 18% thick section, Fig. 1. As indicated, the present CFD results are for a Reynolds number of 3×10^6, while Abbott and von Doenhoff provide data for Reynolds numbers of 3×10^6 and 6×10^6 in the case of a smooth aerofoil, and a Reynolds number of 6×10^6 in the case of a rough aerofoil.

Neither smooth nor rough aerofoils are ideal for comparison with the current, fully turbulent, CFD results across the full range of the angle of attack considered, but it is the only experimental data set available for this section. The key reason for the comparison not being ideal is that whilst the rough aerofoil of the experiment will produce a turbulent boundary layer over the majority of the aerofoil, it will also retard the boundary layer more significantly than will be the case for a turbulent boundary layer on a smooth aerofoil (as we have in the CFD). This increased retardation in turn leads to the pressure coefficients on the suction surface being of smaller magnitude, the result of which is lower lift coefficients for all angles of attack (see for example [6]).

The comparison between CFD and experiment is then as expected: for low angles of attack (up to about 6 degrees) we see good agreement between the CFD and the smooth aerofoil experiment for the lift, and good agreement between the CFD and the rough aerofoil experiment for the drag. For larger angles of attack the agreement deteriorates because both the smooth and rough aerofoil experiments will show stall before the CFD. Overall, and for angles of attack below stall, it is felt the CFD is performing as expected and as intended for both profiles.

D. Variable thickness

Section performance data for a range of thicknesses are shown in Fig. 2. The trends for both the lift and drag coefficients are clear and need little explanation: as the thickness ratio increases the lift-curve slope decreases, the maximum lift decreases and the drag coefficient increases; thus the thicker sections unambiguously behave less well.

E. Alternative coordinate definitions

Unlike other NACA section profiles, such as the 4-digit series, there is no analytical definition of the 6-series section profiles; instead they are derived using an 'inverse' design method whereby the desired pressure distribution is specified and the shape required to achieve such a pressure distribution

[1]The significance of the designation is as follows: the first digit represents the series; the second the chordwise position of the minimum pressure in tenths of the chord; the third (subscripted) the extent of the low drag range in multiples of $0.1c_l$, and which is not know a priori; the fourth the design lift coefficient in tenths; and the fifth and sixth the thickness ratio as a percentage of the chord.

[2]Briefly, $h = 0$ represents the solution extrapolated on to a grid of zero spacing i.e. the continuum value; R is a convergence ratio, for $R < -1$ we have oscillatory divergence, for $-1 < R < 0$ we have oscillatory convergence, for $0 < R < 1$ we have monotonic convergence and for $R > 1$ we have divergence; p is the observed order of convergence and will ideally be close to 2 when we use a second order numerical scheme, but is frequently lower than this; GCI is the Grid Convergence Index and may be though of as a percentage error, with 'm-c' the error for the medium grid and 'f-m' the error for the fine grid; finally, the ratio given in the last column should be close to 1 if we are in the asymptotic region.

TABLE I: Grid convergence study for the 63_x-430: Lift values.

	c_l						GCI		
α	coarse	medium	fine	$h=0$	R	p	m-c	f-m	ratio
0	0.321	0.290	0.282	0.279	0.25	2.00	4.59	1.18	0.97
2	0.548	0.508	0.498	0.495	0.24	2.03	3.18	0.79	0.98
4	0.761	0.707	0.696	0.693	0.21	2.25	2.53	0.54	0.98
6	0.956	0.888	0.868	0.859	0.30	1.75	4.05	1.24	0.98
8	1.122	1.029	0.997	0.981	0.34	1.55	5.85	2.06	0.97
10	1.249	1.120	1.059	1.003	0.48	1.07	13.11	6.63	0.95
12	1.343	1.167	1.055	0.849	0.65	0.63	34.10	24.37	0.90
14	1.435	1.217	1.089	0.907	0.59	0.77	31.86	20.92	0.89
16	1.508	1.262	1.129	0.970	0.54	0.88	28.90	17.54	0.89
18	1.536	1.293	1.168	1.033	0.52	0.95	25.18	14.45	0.90
20	1.528	1.330	1.193	0.885	0.69	0.53	41.80	32.25	0.90

TABLE II: Grid convergence study for the 63_x-430: Drag values.

	c_d						GCI		
α	coarse	medium	fine	$h=0$	R	p	m-c	f-m	ratio
0	0.0169	0.0163	0.0159	0.0131	0.86	0.21	25.07	22.23	0.97
2	0.0178	0.0175	0.0170		2.05				
4	0.0193	0.0198	0.0193		−0.97				
6	0.0223	0.0242	0.0239		−0.19				
8	0.0279	0.0323	0.0324	0.0325	0.03	5.01	0.55	0.02	1.00
10	0.0367	0.0454	0.0466	0.0468	0.14	2.85	3.88	0.52	1.03
12	0.0476	0.0649	0.0678	0.0684	0.17	2.57	6.76	1.09	1.04
14	0.0622	0.0862	0.0884	0.0887	0.09	3.41	3.59	0.33	1.03
16	0.0816	0.1104	0.1118	0.1119	0.05	4.38	1.65	0.08	1.01
18	0.1042	0.1372	0.1349		−0.07				
20	0.1337	0.1683	0.1587		−0.28				

is then calculated. In practice, and when an inverse design program is either unavailable or impractical to use, a thicker section may be scaled from the coordinates for a thinner section, as listed in, e.g. Abbott and von Doenhoff [5].

Thus, three methods (Fig. 3) were identified:

1) Use of an inverse design program, such as that written by Ladson et al. [7]. This might be termed the 'true' method (and was used to produce the coordinates for the verification and validation study as well as the variable thickness study).
2) Scaling of an existing thickness distribution, as published by Abbott and von Doenhoff [5], before addition of the camber line. (This was used with and without modification when comparing sharp and blunt trailing edges.)
3) Scaling of an existing cambered section, with the coordinates again coming from Abbott and von Doenhoff [5].

The significance of different ways of generating a 63_x-430 section profile is shown in Fig. 4. It is clear that the profiles generated by the inverse design method and by scaling of the thickness distribution prior to adding camber behave similarly, whereas the more strongly cambered profile, generated by scaling an already cambered profile, shows a significant shift in the lift curve.

F. 2D blade sections results – sharp and blunt trailing edges

A final aspect of the blade geometry which was investigated was the choice between simulating a sharp and blunt trailing edge. The NACA 6-series sections are defined with a sharp trailing edge whereas in practice tidal turbine blades will have a blunt trailing edge due to manufacturing and structural constraints, with the base thickness being around 1% of the maximum thickness of the section. Such a base thickness is added by linearly increasing the section thickness from the point of maximum thickness.

It was found in this study that the differences between sharp and blunt trailing edge geometries were relatively small, especially for angles of attack below stall. It was also found that the results for the blunt trailing edge geometry at angles of attack around and above the stall angle were particularly sensitive to the grid spacing at the trailing edge, such that a coarse spacing led to results closely resembling those from the sharp trailing edge geometry.

III. BEM RESULTS FOR THE TURBINE

As noted above, the section data of Fig. 2 may be used to improve the Tidal Bladed model of the turbine. For blade stations where the section thickness is less than or equal to 40% the data is interpolated from that shown in Fig. 2 whereas for thicknesses larger than this the data for the 40% thick section is simply used. The results, along with those from

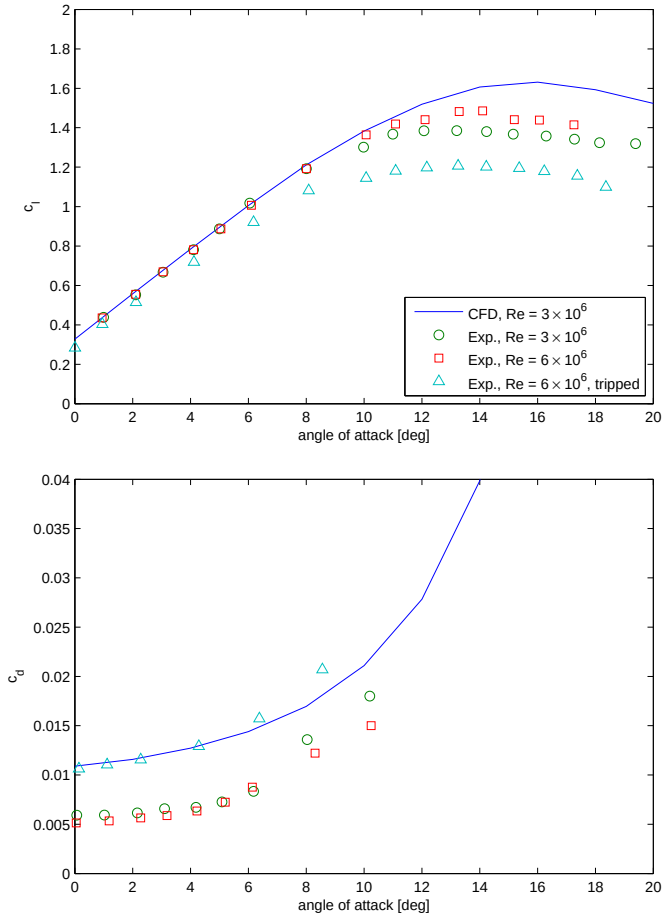

Fig. 1: Coefficients of lift and drag versus angle of attack for the 63_3-418 – comparison of present CFD results (geometry from inverse design method) with data from Abbott and von Doenhoff [5].

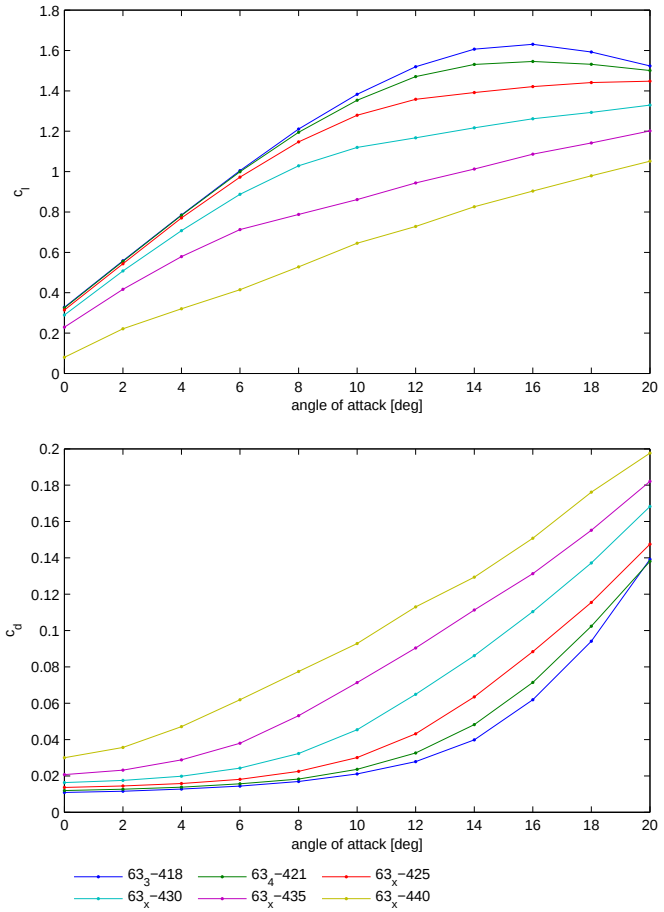

Fig. 2: Coefficients of lift and drag versus angle of attack for various profile thickness rations. All profile coordinates were determined using the inverse design method of Ladson et al. [7].

the 'original' model which used the experimental data for the 63_3-418 section, are shown in Fig. 5. Clearly the difference is significant.

Also shown in this figure are results from Oxford, produced using an in-house BEM code and with section data from Xfoil [8] with tripped boundary layers. (Note that this in-house code has been validated by comparison with Tidal Bladed.) Two predictions are made: the first uses Xfoil data for variable thickness sections which have been scaled from a cambered 63_3-418 section (as discussed above), while the second uses Xfoil data for variable thickness sections produced using the Ladson program. Both of these predictions use section data for thicknesses up to 50%. Again there are significant differences between these two predictions, which shows the importance of the means by which the section coordinates are generated. It might also be noted here that additional results from Oxford have shown that the significant turbine performance degradation relative to the original predictions using 18% thick section data and with natural transition are due to the change to variable thickness section data and to tripped data; neither change alone accounting for the difference in the results.

Overall, it might be concluded that there is significant uncertainty in the turbine performance, but that the present exercise has reduced this uncertainty. The Tidal Bladed predictions using the present CFD data are believed to be the most accurate, based on the quality and relevance of the section data. Finally, the omission of data for sections thicker than 40% is not thought to be significant as these sections occur for small radii where the contribution to the overall rotor performance is minimal due to the comparatively small swept area and lower relative speed of the blade.

IV. Hub and Nacelle Geometry

As discussed previously, the design of the rotor was provided by TGL, whereas no details were provided for what might be termed the 'ancillary geometry'; namely the design of the hub and nacelle. A suitable design for these components was determined by a variety of engineering considerations by workers within the PerAWaT project at the University of Oxford, with input from the present authors. All parameters

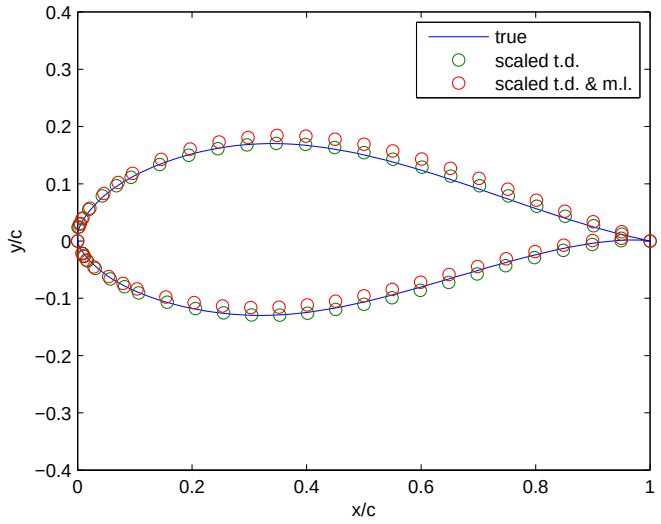

(a)

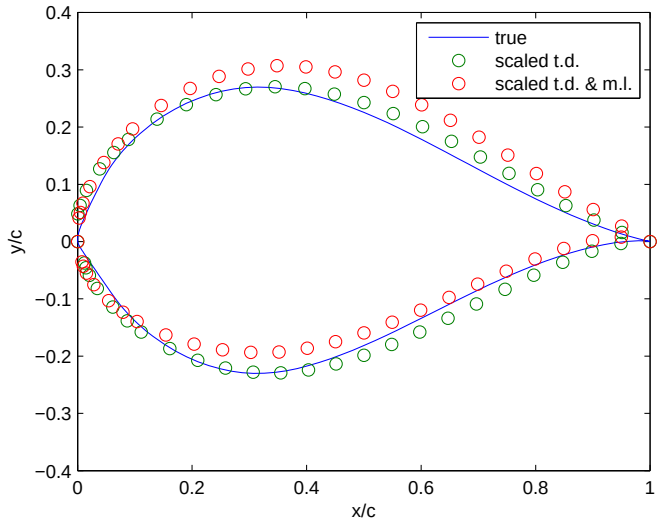

(b)

Fig. 3: Plots of the 63_x-430 and 63_x-450 sections (top and bottom), as derived using three methods: inverse design method (labelled 'true'); scaling of the thickness distribution before adding the camber; and a scaling of a cambered section

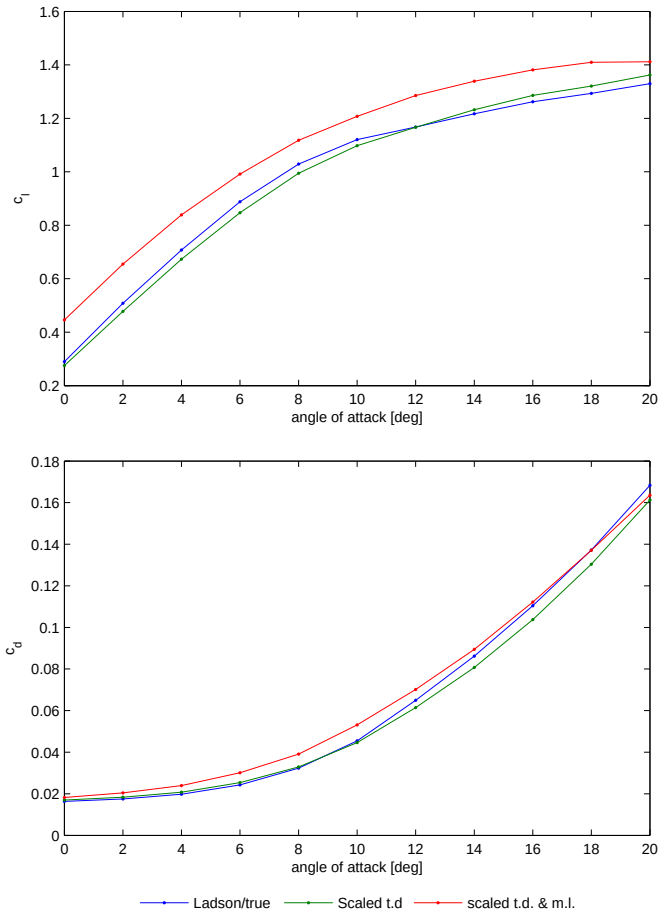

Fig. 4: Coefficients of lift and drag versus angle of attack for a 63_x-430 section, with coordinates derived using three methods (cf. Fig. 3).

TABLE III: Turbine geometry

Parameter	Value
Rotor diameter	18 m
Nacelle diameter	3 m
Nacelle length	5.8 m
Nacelle fillet radius	0.5 m
Hub length	2 m
Nose-cone length	2.25 m
Nose-cone shape	Ellipse, 1:1.5

are noted in Table III and a 3D view of the CAD model is shown in Fig. 6.

Regarding the nacelle, the volume of this was taken to be equal to the volume of a 1 MW Vestas wind turbine, this being 41 m^3. The basic premise here is that the volume of the components contained in the nacelle – primarily the gearbox, generator and transformer – will be related most strongly to the rated power, and so will be equivalent for a 1 MW tidal current turbine. The ratio of diameter to length was set by visual consideration of existing designs, and a cylindrical form was chosen to allow rotating frame of reference CFD simulations to be conducted. A 0.5 m fillet was added at the rear of the nacelle to potentially reduce the nacelle wake. The hub diameter was chosen to match the nacelle while other parameters were again based on visual considerations.

V. CFD RESULTS FOR THE TURBINE

A. Setup

All of the turbine simulations discussed herein were based on the simulation of a single blade of the turbine in a rotating frame of reference and using the SST-k-ω turbulence model. We used a multi-block structured grid with an O-O topology around the blade, details of which are given below.

The computational domain extended 5 turbine diameters (D) upstream of the rotor plane and 40 turbine diameters

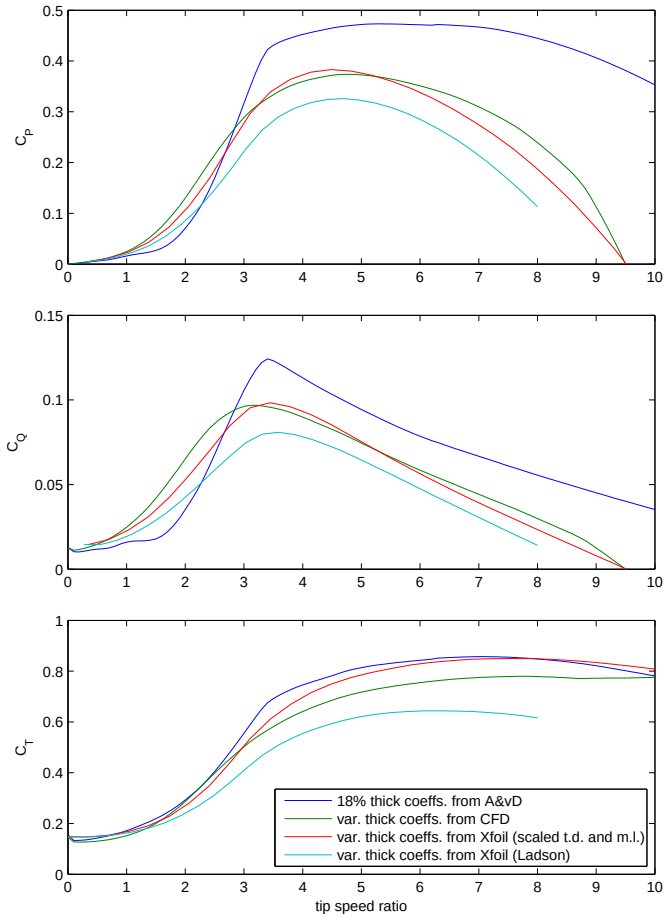

Fig. 5: Coefficients of power, torque and thrust for the turbine, as predicted from Tidal Bladed, using section data for the 63_3-418 from Abbott and von Doenhoff [5] and using section data as per Fig. 2, and as predicted using an in-house BEM code at Oxford with Xfoil data.

downstream. The radial extent of the domain was varied, as discussed later, and was either 2, 4 or 8 turbine radii (R).

Boundary conditions used were as follows: on the inlet (upstream) boundary we specified the velocity, turbulence kinetic energy (k) and turbulence eddy dissipation rate (ϵ); on the outlet the pressure was fixed; on the blade surface and the hub a no-slip condition was specified in the rotating frame; on the nacelle a no-slip condition was specified in the absolute frame. There was also a periodic condition linking the two faces normal to the circumferential direction, while on the 'circumferential' boundary (normal to the radial direction) we again specified an inlet condition for reasons of stability. The inlet condition was a velocity of 2 $\mathrm{m/s}$, with k and ϵ chosen to give a turbulence intensity and length scale of 10% and $1D$ at the rotor plane.

It is worth elaborating on the exact form of the rotating frame of reference model, as this may be formulated in terms of either the relative (to the rotating frame) or absolute (inertial) velocity. We initially worked with the relative velocity form but had serious problems with the boundary conditions;

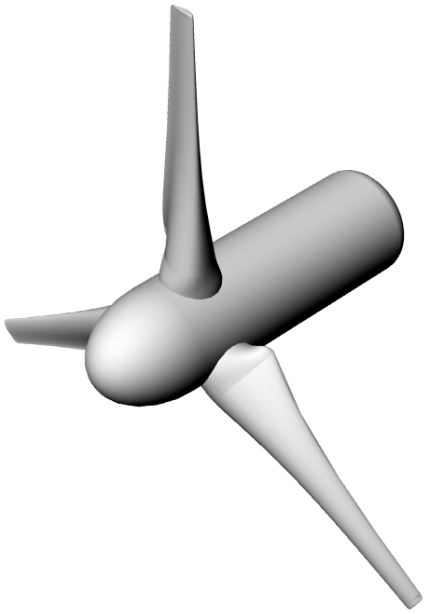

Fig. 6: 3D view of the turbine geometry (excluding tower)

we thus chose to implement the absolute velocity form which solved this problem. Aside from this, it became clear that the absolute velocity form was intrinsically superior for this class of problem (a turbine in a large domain). Given the importance of this choice, and the fact that it is perhaps not especially well know, some details are given below.

B. Relative and absolute velocity formulations of the rotating frame of reference model

The Navier-Stokes equations for the conservation of mass and momentum in an absolute (inertial) frame may be written as:

$$\frac{\partial \rho}{\partial t} + \nabla \cdot (\rho\, \mathbf{u}) = 0$$

$$\frac{\partial}{\partial t}(\rho\, \mathbf{u}) + (\mathbf{u} \cdot \nabla)\rho\, \mathbf{u} = -\nabla p + \nabla \cdot \tau_{ij}$$

where ρ is the density, $\mathbf{u}$ is the velocity vector, p is the pressure and τ_{ij} is the stress tensor.

The relative velocity formulation of the RFR model is arrived at by transforming the above equations to arrive at the following:

$$\frac{\partial \rho}{\partial t} + \nabla \cdot (\rho\, \mathbf{u_r}) = 0$$

$$\frac{\partial}{\partial t}(\rho\, \mathbf{u_r}) + (\mathbf{u_r} \cdot \nabla)\rho\, \mathbf{u_r} + \rho(2\boldsymbol{\omega} \times \mathbf{u_r} + \boldsymbol{\omega} \times \boldsymbol{\omega} \times \mathbf{r}) = -\nabla p + \nabla \cdot \tau_{ij,r}$$

where $\mathbf{u_r}$ is the velocity vector in the rotating frame, ω is the rotational velocity vector of the rotating frame and $\tau_{ij,r}$ is the stress tensor, being based on the velocities in the relative frame. The additional terms, $2\rho\omega \times \mathbf{u_r}$ and $\rho\omega \times \omega \times \mathbf{r}$ are the Coriolis and centripetal accelerations respectively.

The primary disadvantage of this formulation for the problem of a tidal current turbine is that much of the fluid is *non-rotating* in the *absolute* frame, meaning that it is *rotating* in the *rotating* frame. This leads to errors accumulating as the solver attempts to discern small differences between large terms. These issues are discussed in the documentation for commercial CFD codes such as CFX and Fluent; see in particular the Fluent *User's Guide*, Chapter 10, p. 14 [9].

The absolute velocity formulation effects a transformation of the velocity back to the absolute frame for most of the terms; the only velocity term remaining in the relative frame is the so-called *convecting* velocity, as below:

$$\frac{\partial \rho}{\partial t} + \nabla \cdot (\rho\, \mathbf{u}) = 0$$

$$\frac{\partial}{\partial t}(\rho\, \mathbf{u}) + (\mathbf{u_r} \cdot \nabla)\rho\, \mathbf{u} + \rho(\omega \times \mathbf{u}) = -\nabla p + \nabla \cdot \tau_{ij}$$

Note that the Coriolis and centripetal terms are modified to a single term.

This formulation can be achieved in Code_Saturne by making use of subroutines developed to handle moving grids.

C. Computational grids

Chord-wise and wall-normal grid spacings on the turbine blade are based on those used for the 2D blade sections. Cell-counts are 96 chord-wise with an additional 4 on the blunt trailing edge, and 26 within the boundary layer blocks (which extend to $0.1c$). Note that we adopt the 'coarse' grid spacing of the blade sections as the default spacing for the turbine for reasons of computational cost.

Span-wise spacings are as follows. For the main section of the turbine blade (from $r = 2.05$ m to $r = 8.85$ m)) we use a spacing of 0.075 m at the minimum radius and 0.025 m at the maximum radius with stretching ratios limited to 1.1 in between, this giving 52 cells. For the root blocks there are a total of 30 cells span-wise (24 of which are in the hub boundary layer). The tip block has 10 cells span-wise to give a minimum spacing of 0.0033 m at the tip. Stretching ratios are again less than 1.1. Note that the spacing of 0.0033 m span-wise is approximately equal to the chord-wise spacing towards the leading edge at the tip.

Given the nature of multi-block structured gridding, the above specification of chord-wise, wall normal and span-wise spacings largely pre-determined the rest of the grid. One point to note is that maximum aspect ratios were chosen as 20 at the boundaries and 50 within the domain, this being based on the best practice guidelines of e.g. Casey and Wintergerste [10, pp. 82–3]. Total cell counts were around 2×10^6 depending on the degree of coarsening in the wake and the radial extent while computational run times were between 1000-2000 CPU hours depending on the grid. A view of the blocking and mesh is shown in Fig. 7.

D. Verification of the grid spacing in the turbine wake

Verification of the computational solution was achieved by simultaneously investigating the effect of iterative convergence and the effect of the grid spacing in the wake of the turbine. Three grids were used for this, all with radial boundary at $2R$, the key differences being that the first used relatively fine grid spacing throughout the downstream region, while the second and third used relatively coarser spacing from, respectively, 10 diameters and 1 diameter downstream of the turbine.

The solution parameters which were monitored were as follows: in respect of the iterative convergence the power and thrust coefficients were monitored as well as the streamwise velocity at a number of streamwise locations on a profile at $y/R = 0.5$ and $z = 0$ (i.e. a line intersecting the mid-span of the blade); in comparing the solutions from the three grids once iterative convergence was deemed to have been achieved we examined longitudinal and lateral profiles of the streamwise velocity. See Fig. 10 for a view of these profiles.

In general, it was found that for the power and thrust coefficients, iterative convergence was achieved after as few as 500 iterations, with the solution being the same for all of the grids used. For the velocity probes in the wake, and the wake profile, full convergence took a much larger number of iterations and showed a slight sensitivity to the grid spacing in the wake. We therefore decided to employ the grid where coarsening was introduced at $x/D = 10$ as this offered slightly greater fidelity in the near wake, and to run simulations for 4000 iterations to ensure iterative convergence.

E. Parametric study of the effect of the domain radius

Following the verification of the iterative convergence and the grid, we proceeded to investigate the effect of the radial extent of the domain on the power and thrust coefficients and the streamwise velocity profiles. This study utilized three grids, the first with a circumferential boundary at $2R$, as above, and the second and third with a circumferential boundary at $4R$ and $8R$ respectively.

As with the first part of the verification, we again conducted an investigation into the iterative convergence of the power and thrust coefficients and the streamwise velocity at a number of locations, as shown in Figs. 8 and 9. Considering first the power and thrust coefficient, we see that the convergence is somewhat slower for the larger domains (that is, the domains with circumferential boundary further from the turbine). Nevertheless, it is clear that convergence is achieved after about 1000 iterations.

For the streamwise velocities in the wake, the pattern of convergence is similar, but as the wake extends a greater distance downstream when the effect of blockage is lower, it takes a much larger number of iterations to ensure full convergence. (As is shown, all solutions, including that from the previous section, were advanced to $12\,000$ iterations to thoroughly investigate the effect of convergence.) We may

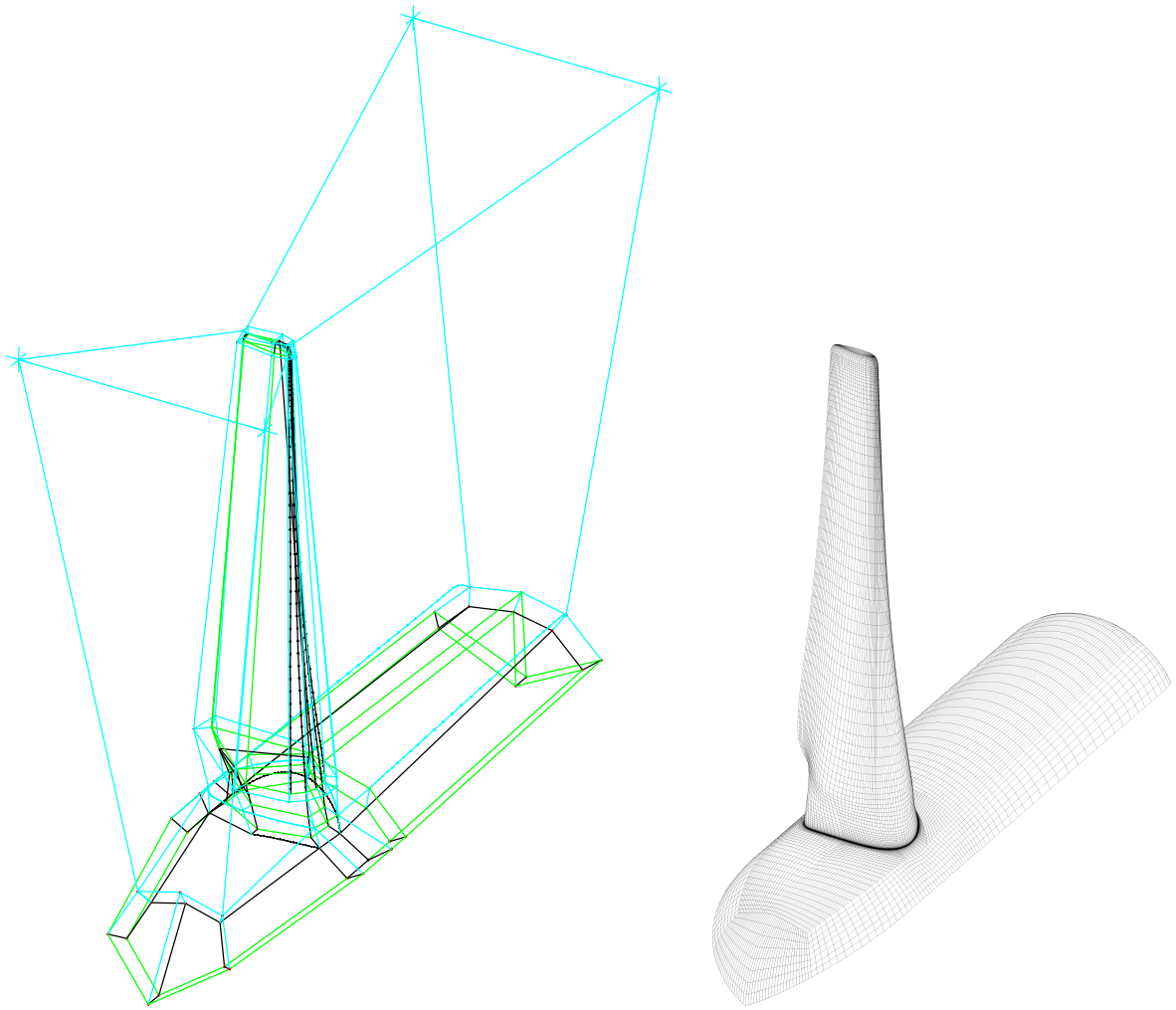

(a) (b)

Fig. 7: Views of the blocking around the blade, hub and nacelle (left) and the completed surface mesh on the afore-mentioned parts.

conclude that in order to get an accurate solution for the wake up to 16 diameters downstream of the turbine – by which point the deficit velocity is less than 10% of the free stream for all domain sizes – we need to run the simulations for $6\,000$ iterations.

Considering the effect of the domain radius on the power and thrust coefficients, it can be seen from Fig. 8 and Table IV that as the radius increases both coefficients decrease monotonically. This is in line with analytical blockage corrections (see for example [11]). It can also be seen that the change from the $2R$ grid to the $4R$ grid is much more significant than that from the $4R$ grid to the $8R$ grid. Both of these features are as expected and can clearly be parameterized based on the existing results.

The effect of the domain radius on the velocity profiles is shown in Figs. 11 and 12. Clearly for the domains with less blockage the velocity deficit is greater (lower velocity in the wake core) and the speed of the bypass flow is lower. Again, this is as per analytical blockage corrections. We also see that wake recovery is slower when the blockage is decreased. This latter feature is not (and cannot) be predicted by the aforementioned analytical blockage corrections, but can be readily explained: as the bypass flow is slower for cases with lower blockage ratios, the velocity gradients will be smaller, which in turn will produce less mixing and therefore the slower wake recovery. Again, it can be seen that the change from the $2R$ grid to the $4R$ grid is much more significant than that from the $4R$ grid to the $8R$ grid. This would suggest that blockage effects are most significant for domain radii below $4R$.

VI. Conclusions

This paper describes the creation and verification of a computational fluid dynamics (CFD) model of a horizontal axis tidal current turbine that can be used to parameterize the wake from the turbine.

Following verification and validation of the CFD model of the blade sections, we have shown the dependence of the section performance on the thickness ratio and the method of

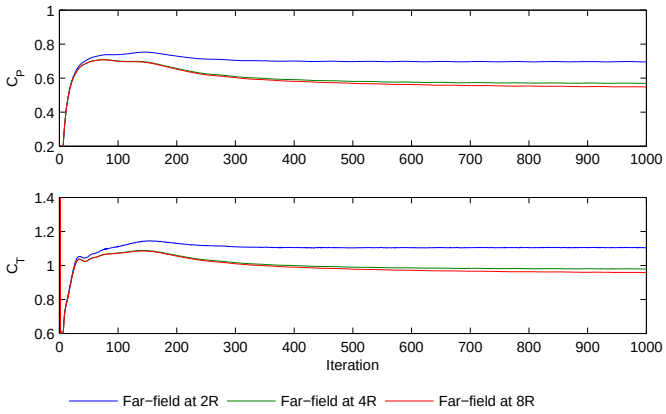

Fig. 8: Iterative convergence of the power and thrust coefficient for the domain radius study.

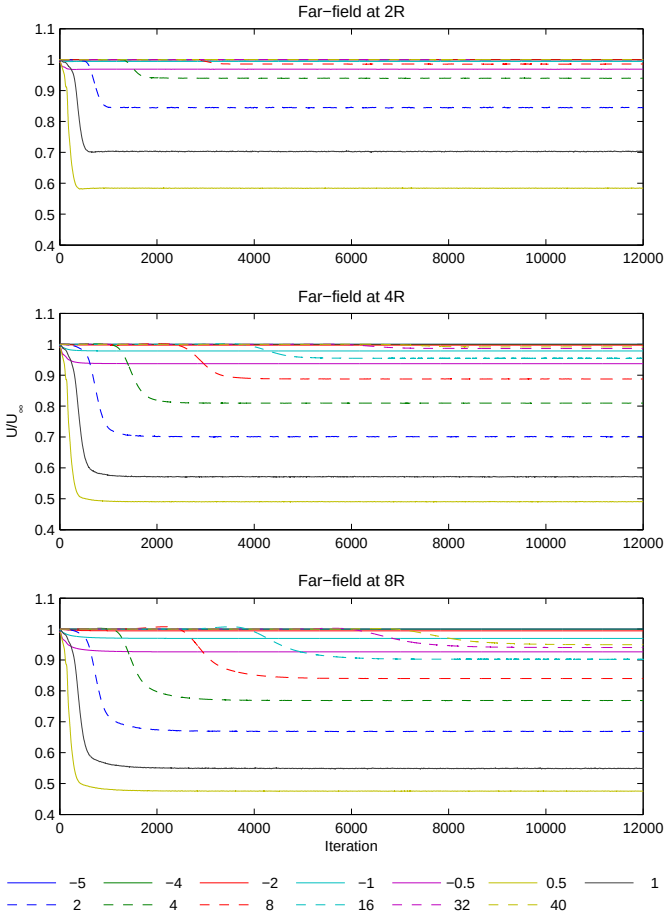

Fig. 9: Iterative convergence of the streamwise velocity at different probe positions for the domain radius study.

TABLE IV: Power and thrust coefficient results from the domain radius study, with percentage differences from the results on the $8R$ mesh shown in parenthesis. Values after 6 000 iterations.

	Domain extent					
	$2R$		$4R$		$8R$	
C_P	0.698	(+28.78%)	0.569	(+4.98%)	0.542	(–%)
C_T	1.107	(+17.52%)	0.980	(+4.03%)	0.952	(–%)

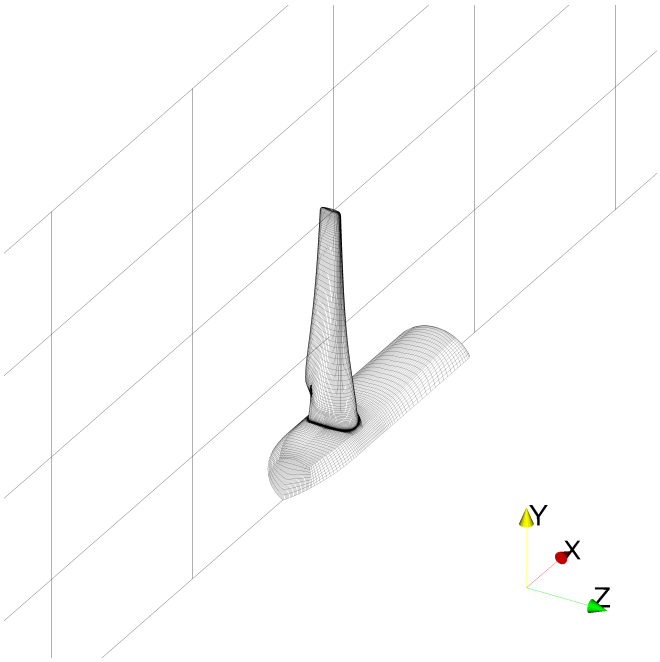

Fig. 10: Locations of the 1D profiles. The five longitudinal (x-direction) profiles at $y/R = 0.0$, 0.5, 1.0, 1.5 and 2 are shown as well as the lateral (y-direction) profiles at $x/D = -1.0$, -0.5, 0.0, 0.5 and 1.0.

generating the section coordinates. It has also been shown that the blade sections with sharp and blunt trailing edges behave similarly below stall. These results, along with results from Xfoil, have been used to investigate the turbine performance using a BEM model. Concluding the preliminary work towards the CFD model of the turbine we have outlined the creation of a generic hub and nacelle geometry.

The development of the CFD model of the turbine has been outlined in later sections and results have shown the importance of the radial extent of the computational domain, this representing the blockage ratio. Finally, and as noted in the introduction, we conclude by noting that this model of the turbine will be used to parameterize the wake in future work.

ACKNOWLEDGEMENTS

The work described in this paper has been carried out as part of the PerAWaT project, commissioned by the Energy Technologies Institute (ETI).

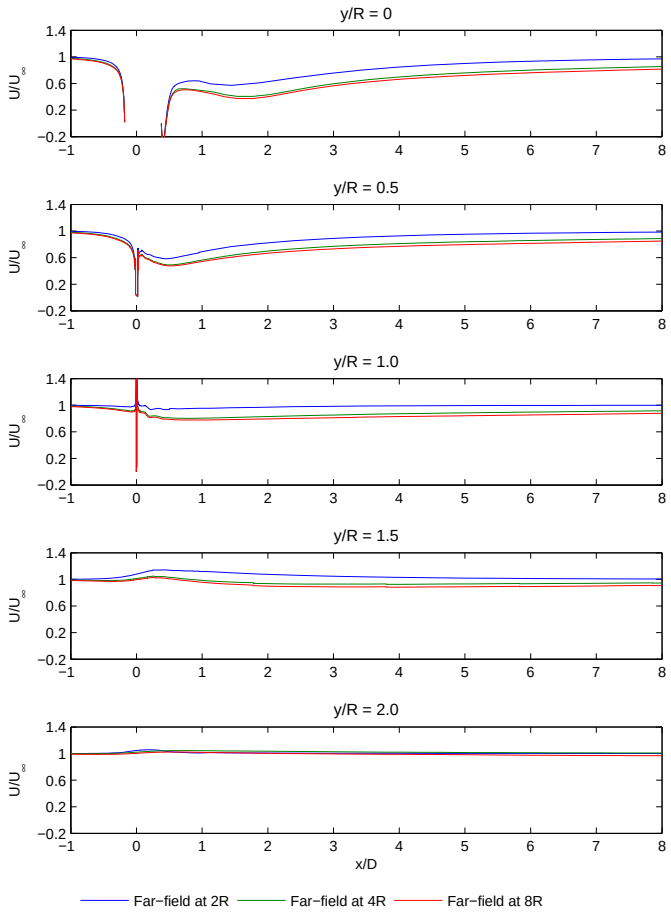

Fig. 11: Longitudinal profiles of the streamwise velocity at five lateral positions after 12 000 iterations.

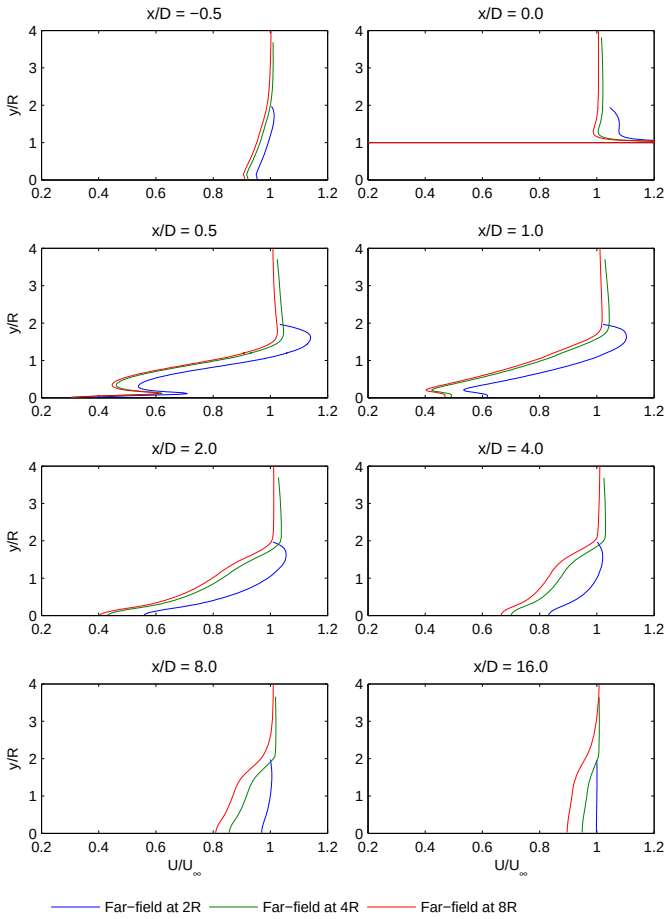

Fig. 12: Lateral profiles of the streamwise velocity at eight longitudinal positions after 12 000 iterations.

As noted in the paper, contributions to the present work were made by those working within the PerAWaT project at the University of Oxford, principally Simon McIntosh and Richard Willden.

References

[1] Robert Rawlinson-Smith, Ian Bryden, Matt Folley, Vanessa Martin, Tim Stallard, Clym Stock-Williams, and Richard Willden. The PerAWaT project: Performance assessment of wave and tidal array systems. In *Proceedings of the 3rd International Conference on Ocean Energy*, Bilbao, Spain, 2010.

[2] Gareth I. Gretton. *The hydrodynamic analysis of a vertical axis tidal current turbine*. PhD thesis, School of Engineering, University of Edinburgh, 2009.

[3] Patrick J. Roache. *Verification and Validation in Computational Science and Engineering*. Hermosa, Albuquerque, New Mexico, USA, 1998.

[4] NPARC. *Examining spatial (grid) convergence*, 2008. URL http://www.grc.nasa.gov/WWW/wind/valid/tutorial/spatconv.html. [Accessed 4th February 2009].

[5] Ira H. Abbott and Albert E. von Doenhoff. *Theory of Wing Sections*. Dover, 1959.

[6] N. Gregory and C. L. O'Reilly. Low-speed aerodynamic characteristics of NACA 0012 aerofoil section, including the effects of upper-surface roughness simulating hoar frost. Aero Report 1308, NPL, 1970.

[7] Charles L. Ladson, Cuyler W. Jr. Brooks, Acquilla S. Hill, and Darrell W. Sproles. Computer program to obtain ordinates for NACA airfoils. Technical Memorandum 4741, NASA, 1996.

[8] M. Drela and H. Youngren. *Xfoil 6.9 User Primer*, 2001. URL http://web.mit.edu/drela/Public/web/xfoil/.

[9] Ansys Inc. *ANSYS Fluent 12.0 User's Guide*, 2009.

[10] Michael Casey and Torsten Wintergerste. *Special Interest Group on Quality and Trust in Industrial CFD: Best Practice Guidelines*. ERCOFTAC (European Research Community on Flow, Turbulence and Combustion), 2000.

[11] A. S. Bahaj, A. F. Molland, J. R. Chaplin, and W. M. J. Batten. Power and thrust measurements of marine current turbines under various hydrodynamic flow conditions in a cavitation tunnel and a towing tank. *Renewable Energy*, 32:407–426, 2007.